

Near Earth Objects and Their Physical Characterization

Jean-Baptiste Kikwaya Eluo, S.J.

Abstract The present research on Near Earth Objects (NEOs) is mostly limited on addressing the question on their number and how hazardous they may be to the Earth. Catalina Sky Survey (CSS) has submitted thousands of astrometric observations to the Minor Planet Center (MPC) resulting in discovery of hundreds of NEOS but much of their physical characteristics remain unknown. OSIRIS-Rex, a return sample mission, will visit 1999 RQ36, a carbonaceous asteroid, physical characteristic which could only be identified through other techniques of observations than just astrometry. Using VATT (Vatican Advanced Technology Telescope), we observed 11 NEOs using photometry with four broadband filters (BVRI). With this project where we combined two approaches (two-color plots, and comparison of relative reflectance normalized to V-filter with the real observed spectra), we were able to determine color of the 11 NEOs, and therefore had some clue about their physical characteristics particularly composition, size, structure, albedo...

Introduction

Until a few years ago, research on Near Earth Objects (NEOs) was solely oriented toward addressing the question of their number and how hazardous they might be to the Earth. For example, since 1998 the Catalina Sky Survey (CSS) has been searching for NEOs using 68/76 cm f/1.9 classical Schmidt optics capable of going down to 20.5 magnitude, and it has submitted thousands of astrometric observations to the Minor Planet Center (MPC) resulting in discovery of hundreds of NEOs. But much of their physical characteristics remain unknown. On the other hand, OSIRIS-Rex, a return sample mission launched on October 8th, 2016, will visit 1999 RQ36, an NEO asteroid (asteroid Bennu) which is thought to be a carbona-

J.-B. Kikwaya Eluo, S.J. (✉)
Vatican Observatory, Tucson, AZ 85721, USA
e-mail: jbkikwaya@gmail.com

aceous asteroid: a physical characteristic that could only be identified through other techniques of observation than just astrometry.

Asteroids are the building blocks of terrestrial bodies (Mercury, Venus, Earth, and Mars), and possibly also of the cores of the giant planets (Jupiter, Saturn, Uranus, and Neptune). They conserve the signature of the presolar nebula in which the planets formed. They can also inform us on how life started on Earth since they might contain the original organic matter and water. In fact, we know now, thanks to Rosetta mission, comets might probably not be the source of Earth's water. There is then a real need to focus on asteroids, which must be studied in order to answer questions related to the origin of water and life on Earth. And that can be accomplished when we begin to study the physical characterization of asteroids.

As asteroids carry the signature of the birth of the solar system, they are able to help us also to understand how many stars injected their matter into early solar system and what kind of stars they might be. As we gather observed compositional and structural properties of asteroids, we enable ourselves more and more to build new theories to explain the different processes that brought the solar system from its initial state to the present one. This knowledge can also allow us to infer what is happening in other solar systems at different stages of their evolution.

The most accurate method to study the physical characterization of asteroids is to use spectroscopy that covers both the optical and near-infrared electromagnetic spectrum to obtain their reflectance spectra, and thermal infrared emission to estimate their albedo (Dandy et al. 2002). This method not only is time-consuming, but it is also very expensive.

A very straight forward and inexpensive method is to use optical photometry with a set of very broad band filters from Blue to Infrared (BVRI) (Landolt 1992). The four main asteroid spectral classes from the Tholen classification (C, D, M, and S) are easily obtained with this method (Zellner et al. 1985). C represents dark carbonaceous asteroids. D groups all those asteroids with low albedo. They contain organic-rich silicates, carbon, and possibly water ice. They are found mostly in the outer asteroid belt and beyond. Class M is a class of metallic asteroids. All "stony" asteroids are put together in class S.

In 2014 we started a program of observing NEOs using the Vatican telescope at Mt Graham in Arizona in USA. Our project consists in determining the physical characterization of NEOs. We use photometry with 4 broadband Johnson-Cousin filters. To determine the surface color of a particular NEO, we use the two color plots of three different color indices (B-V, V-R, and V-I) (Zellner et al. 1985). This method, as a first approach, helps to estimate the optical color of asteroids in general, and NEOs in particular (Dandy et al. 2003; Yoshida et al. 2004). In our work, we take this method one step further by creating from these color indices a very broad spectrum normalized at V color for each NEO, which we compare with real observed spectra in our database through the program "modeling for asteroids" by Birlan Mirel (Popescu et al. 2012). In this way, more information becomes available to describe physically each NEO than what the two-color plots alone can provide from optical photometry.

Instrument and Data

We use Vatican Advanced Technology Telescope (VATT) for gathering our data. VATT is an f/1.0 telescope with a primary mirror of 1.8 m in diameter. Its secondary mirror is f/0.9 with a diameter of 0.38 m. For photometry and astrometry, we use a new STA0500A back illuminated 4K CCD camera with a resolution of 4064×4064 pixels on $15 \times 15 \mu\text{m}$. Without binning, the pixel scale is 0.188 arcsec/pixel and the image reading time is 60 s. For our project on NEOs, we set the CDD to bin two by two in order to reduce the readout time to 30 s. Consequently, the resolution dropped to 2016×2016 pixels and the pixel scale to 0.375 arcsec/pixel. The wavelength range covers the entire visible spectrum (300–1000 nm). The quantum efficiency of the instrument (VATT 4K) peaks at 450 nm.

Our project consists in observing those NEOs thought to have a fast spin rate (fast rotators). To ensure that we observe fast rotators, we aim at those asteroids with high absolute magnitude ($H > 22$) as they tend to be small, on the order of several dozen meters (Fedorets et al. 2017; Tricarico 2017; Schunova-Lilly et al. 2017). We collected 11 NEOs from 2014 to 2016 with H ranging from 21.5 to 27. They are 2014 AY28, 2014 EC, 2014 KS40, 2014 WF201 observed with only three filters (B, V, and R), 2015 FP with only two filters (V, and R), 2015 TB25, 2015 VM64, 2015 VT64, 2015 XZ1, 2016 EW1, and 2016 GW221 observed using four different filters (B, V, R, and I).

We will describe in great detail NEO 2014 WF201 (Fig. 1), and for others, we will only give the final results as we use the same technique to observe, reduce, and analyze them. 2014 WF201 was announced by the Minor Planet Center on November 24th, 2016. Its absolute magnitude was 25.6. Its delta distance (its closest distance to the Earth) was 0.018 AU (astronomical distance, distance between the Sun and the earth being 1 AU) when being at 1.005 AU from the Sun. We observed it the night of November 25th, 2016 and November 26th, 2016. We took 85 frames with the R-filter to cover its complete lightcurve in order to estimate its spin rate. For color, we observed 2014 WF201 with three more filters. We took 5 frames in the B-filter, 5 frames in the V-filter, and 5 frames the I-filter with the following sequence: R-B-R-V-R-I-R: 15 frames in R, 5 frames in B, 15 frames in R, 5 frames in V, 15 frames in R, 5 frames in I, and 40 frames in R. The details for the other 10 NEOs are reported in Table 1.

Reduction and Analysis

For each campaign run, we took nearly 200 bias frames, and using the IRAF packages *imred*, *ccdred*, and *zerocombine* (Tody 1986) we created a master bias frame to be used in the calibration of the science frames. We also took 50 flat frames in each filter. One master flat in each filter was then created using the IRAF packages *imred*, *ccdred*, and *flatcombine* (Tody 1993). For the calibration of the

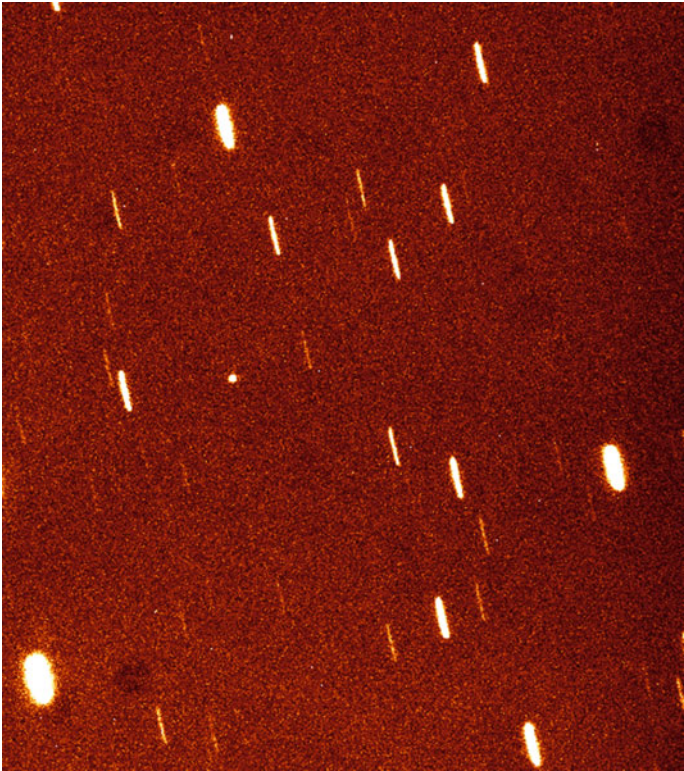


Fig. 1 NEO 2015 WF201 appears as a dot. Stars are trailed because the image was taken following the bias rate of the object (motion of the object on the sky)

Table 1 11 NEOs, dates of observation, number of frames for each filter (R, B, I, and V), object absolute magnitude (H), distance from the Earth, and distance from the Sun as released by Minor Planet Center

Asteroid	Date of observation	R-filter	B-filter	I-filter	V-filter	H	Delta (AU)	r (AU)
2014AY28	2014 04 05	42	5	–	7	21.8	0.071	1.024
2014EC	2014 03 05	40	50	–	50	28.2	0.017	1.009
2014KS40	2014 06 01	50	15	–	10	21.9	0.068	1.065
2014WF201	2014 11 26	85	5	5	5	25.6	0.018	1.005
2015FP	2015 03 24	75	–	–	15	25.2	0.031	1.027
2015TB25	2015 10 14	135	10	10	10	24.5	0.027	1.019
2015VM64	2015 11 09	50	4	4	4	26.1	0.025	1.015
2015VT64	2015 11 09	60	5	6	5	26.0	0.025	1.015
2015XZ1	2015 12 08	20	5	5	5	25.0	0.043	1.028
2016EW1	2016 03 07	45	4	4	4	25.2	0.028	1.017
2016GW221	2016 05 03	45	5	5	5	24.8	0.048	1.049

science frames observed with one particular filter, we applied master bias and master flat of the same filter to them using the IRAF packages `imred`, and `ccdproc`.

For the photometry reduction, we used the IRAF packages `ccdphot`, `digiphot`, `apphot`. For one particular frame, we detected the dot representing the object, we used the IRAF command `imexam` combined with the `r-key` to get the object profile that gives among other characteristics of the object its full width at half maximum (FWHM). We set the aperture for the photometry to twice this value with the IRAF command `photpars.aperture = (2 * FWHM)`. The IRAF command `phot` followed by the name of the frame fits file gives, the time that frame was captured in UT, the magnitude of the object on that particular frame, the error in magnitude, the exposure time, the airmass, and the pixel value of the sky.

We also observed standard stars to correct for the fact that we can't use the differential photometry, as the stars in the field don't appear as point sources due to our observation settings. We take 4–5 standard stars observed with each of the four filters. After applying bias and flat calibration, we calculate total magnitude of each standard star as:

$$\begin{aligned} \text{Total magnitude} &= \text{Standard star catalog magnitude} \\ &\quad - \text{Standard star Instrumental magnitude} \end{aligned}$$

We plot total magnitude of the standard stars versus their air masses and make a linear fit whose slope is the extinction coefficient. Typical extinction coefficients for VATT4K are 15% for B-filter, 10% for V-filter, 8% for R-filter, and 5% for I-filter. To apply the standard stars correction to the science frames, we use the zero point and the slope from the linear fit. The magnitude of the object on each frame is modified as:

$$\begin{aligned} \text{Object magnitude on one frame} &= (\text{zero point magnitude} + \text{object instrumental magnitude}) \\ &\quad - \text{object airmass} \times \text{extinction coefficient} \end{aligned}$$

We obtain as many magnitude measurements of the object as the number of frames in each of the four filters. We used ALC (Asteroid Light Curve), an Asteroid Lightcurve Analysis Program, to compute both the lightcurve and the color indices of the object (Pravec, x). We begin by displaying the frames taken with the R-filter. When the B-filter frames are displayed, there is an offset with the R-filter, which is the color index R-B. We adjust the B-filter object measurements to the R-filter ones. And we proceed with the V-filter, and I-filter to have the color indices R-V, and R-I. We transform these color indices to B-V, V-R, and V-I as the two color plots are B-V versus V-R, and V-I versus V-R (Table 2). The error bar in each filter is generated from the lightcurve fit to data.

For each NEO, we computed the absolute magnitude using its orbital elements (semi-major axis, eccentricity, inclination, perihelion, and period) (Table 3). We placed the 11 NEOs in the *a-e* plot as suggested by Dandy et al. 2003 where Aten, Apollo, Amor, and Jupiter family comets ($2 < T < 3$) defined by Bottke et al.

Table 2 11 NEOs with their color indices V-R, B-V, and V-I that help to make the two color plots in order to estimate in a very broad and first approach the surface color of the asteroids: type C, type D, type M, and type S (Zellner et al. 1985)

Asteroid	V-R	d(V-R)	B-V	d(B-V)	V-I	d(V-I)
2014AY28	0.32	0.045	0.793	0.051	–	–
2014EC	−0.052	0.099	0.567	0.087	–	–
2014KS40	0.445	0.053	0.595	0.052	–	–
2014WF201	0.399	0.036	0.795	0.062	0.688	0.041
2015FP	0.258	0.051	–	–	–	–
2015TB25	0.338	0.052	0.805	0.052	0.694	0.054
2015VM64	0.315	0.047	0.768	0.044	0.751	0.046
2015VT64	0.333	0.044	0.895	0.054	0.626	0.053
2015XZ1	0.365	0.055	0.732	0.041	0.695	0.051
2016EW1	0.42	0.041	0.733	0.051	0.62	0.041
2016GW221	0.343	0.048	0.775	0.042	0.708	0.042

Two NEOs, 2014 EC and 2015 FP, are particularly of great interest as their color indices fall outside the ranges

Table 3 Orbital elements of the 11 NEOs as given by Minor Planet Center

Asteroid	Semi-major axis (AU)	Eccentricity	Inclination (°)	Perihelion (AU)	Period (year)
2014AY28	1.425	0.283	5.709	1.023	1.70
2014EC	1.459	0.526	1.403	0.691	1.76
2014KS40	2.294	0.538	2.924	1.060	3.47
2014WF201	1.109	0.109	8.505	0.988	1.17
2015FP	1.550	0.348	9.712	1.010	1.93
2015TB25	1.282	0.208	16.915	1.016	1.45
2015VM64	1.886	0.619	16.311	0.718	2.59
2015VT64	1.166	0.171	17.988	0.967	1.26
2015XZ1	1.089	0.179	19.827	0.894	1.14
2016EW1	1.038	0.268	18.898	0.760	1.06
2016GW221	0.827	0.268	3.655	0.605	0.75

(2002) are well marked. Different taxonomy types tend to occupy different regions of (a, e) space (Dandy et al. 2003). The (a, e) plot also gives an indication of the source of NEOs.

NEOs belonging to Amor region with $a > 2$ or near 2.5 are believed to be delivered to the Earth through the 3:1 resonance with Jupiter (Bottke et al. 2002) while those from Apollo and Aten regions reach the Earth through the v6 secular resonance. It happens that the 3:1 and v6 resonances are very “fast track” in the delivery of NEOs to the Earth (Bottke et al. 2002). Only $\sim 10^6$ years are needed for an object, entering this region as result of collision, to be delivered to the Earth (Froeschle et al. 1995; Rabinowitz 1998). We expect then that these NEOs would

keep some freshness of their surface when they reach the Earth. And they tend to belong to D-type (also V-type, and R-type not described in this work). Their spectra show a deep 1- μ m absorption band (Dandy et al. 2003).

NEOs from an IMC (Intermediate Mars-Crossing) source follow a very slow track of delivery (Rabinowitz 1997) as they take about 10^9 years to reach the Earth. As result, they experience more the effect of space weathering. They tend then to be S-type (Dandy et al. 2003).

C-type NEOs seem to come from all over the place. Some place them among Amors with $A > 1.5$ AU and Apollos with moderate eccentricity (Dandy et al. 2003). We found them in the main belt from the central to the outer region where the delivery mechanism is dominated by the 3:1 resonance (Bottke et al. 2002). But they are also present in the region with a < 2 where we expect to find E or M-types (Dandy et al. 2003).

Results and Discussion

Lightcurve and Spin Rate

2014 WF201 lightcurve (Fig. 2) computed using ALC software determined its spin rate that is 1.00 ± 0.03 h. With this small rotation period, 2014 WF201 is considered to be a fast rotator. Error on each observed point of the lightcurve is estimated by combining error from the reduction and the one from the fit.

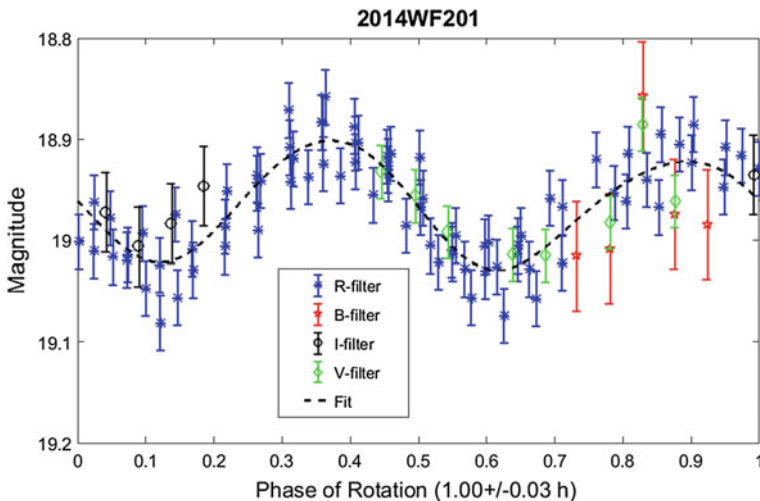


Fig. 2 Lightcurve of neo 2014 WF201. The object came very close to the Earth at 0.018 AU

Table 4 Spin rates of the 11 NEOs

Asteroid	Rot. period (h)	Amplitude (mag)
2014AY28	1.88 ± 0.03	0.32 ± 0.04
2014EC	0.56 ± 0.01	0.48 ± 0.16
2014KS40	0.98 ± 0.04	1.26 ± 0.16
2014WF201	1.00 ± 0.03	0.13 ± 0.02
2015FP	0.17 ± 0.01	0.51 ± 0.06
2015TB25	0.67 ± 0.04	0.31 ± 0.08
2015VM64	2.30 ± 0.03	0.23 ± 0.07
2015VT64	1.13 ± 0.01	0.40 ± 0.13
2015XZ1	0.95 ± 0.07	0.33 ± 0.09
2016EW1	1.34 ± 0.02	1.40 ± 0.03
2016GW221	0.29 ± 0.05	0.41 ± 0.10

For the 10 other objects, we give only their spin rates that range from 0.17 ± 0.01 h to 2.30 ± 0.03 h (Table 4) and the amplitudes of the lightcurves from 0.23 ± 0.07 mag to 1.40 ± 0.03 mag.

Two Color Plots

In order to determine the color of any NEO in a very first approach, we used two color plots (V-R, B-V) and (V-R, V-I) from the work of Zeller et al. (1987) which gives the four main optical types of asteroids (C-type, D-type, M-type, and S-type). The two color plots of 2014 WF201 show that it belongs to the C-type. In fact,

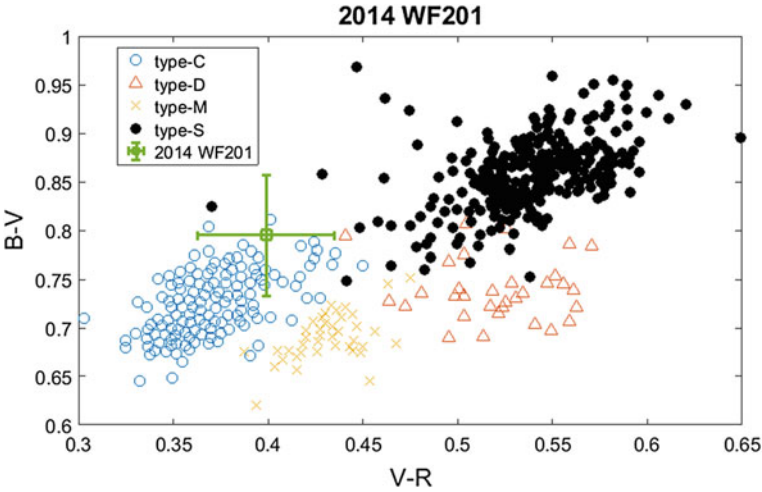


Fig. 3 NEO 2014 WF201 is a C-type asteroid

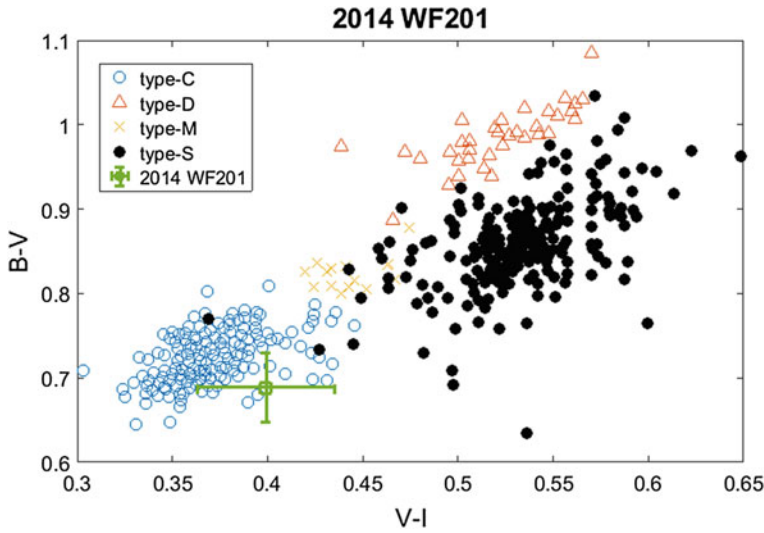


Fig. 4 NEO 2014 WF201 falling among C-type asteroids is therefore a C-type object

in the two color plot B-V versus V-R, 2014 WF201 falls with C-type asteroids (Fig. 3), and this is confirmed by the two color plot V-I versus V-R where 2014 WF201 is also among C-type asteroids. For the 10 other objects, 6 are clearly C-type, one is either C-type or S-type, two from this method cannot be unequivocally classified, and one, being observed only with two colors (V, and R) cannot be placed in the two color plots (Fig. 4).

Relative Reflectance and Spectra

From the color indices (V-R, B-V, and V-I), we computed reflectance values normalized to V of the 11 NEOs and we compared them with the observed spectra in database using the program “modeling for asteroids” by Birlan Mirel (Popescu et al. 2012). When comparing the optical relative reflectance of 2014 FW201 (Fig. 5) with spectra in the database, three different spectra match it (Figs. 6, 7 and 8). It turns out that 2014 WF201, which was optically described as C-type, can actually now be classified as Cg, Cgh (C-complex classes that are refined classes of carbonaceous asteroids) (Popescu et al. 2016). One representative of these classes is asteroid 1 Ceres. 2014 WF201 might also be an O-type, a very rare class of asteroids. The spectra of O-type asteroids match those of L6 and LL6 ordinary chondrite meteorites (Bus and Binzel 2002a, b).

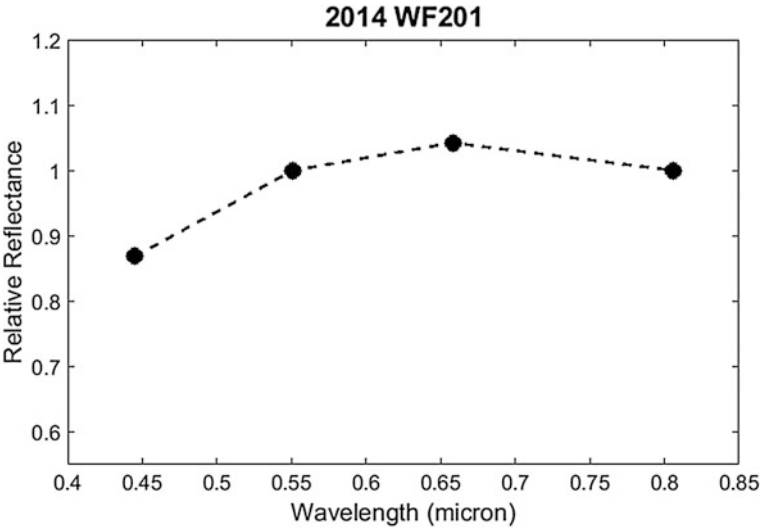


Fig. 5 Optical reflectance of NEO 2014 WF201

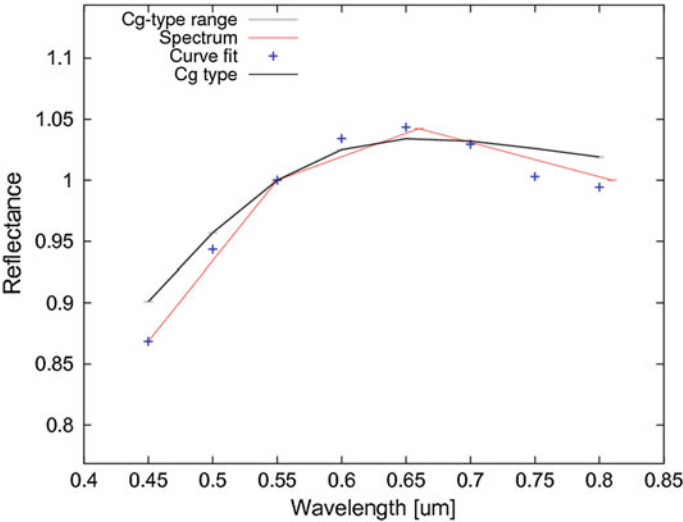


Fig. 6 Optical reflectance of 2014 WF201 matches Cg-type spectra

Among the 11 NEOs, only three (2015 FP, 2014 KS40, 2014 EC) could not have their reflectance matching spectra in the database. Beside classes Cgh, Cg, and O, optical reflectance of 2015 VM64 matched spectra of Ch asteroids (Ch belongs also to C-complex classes) (Table 5).

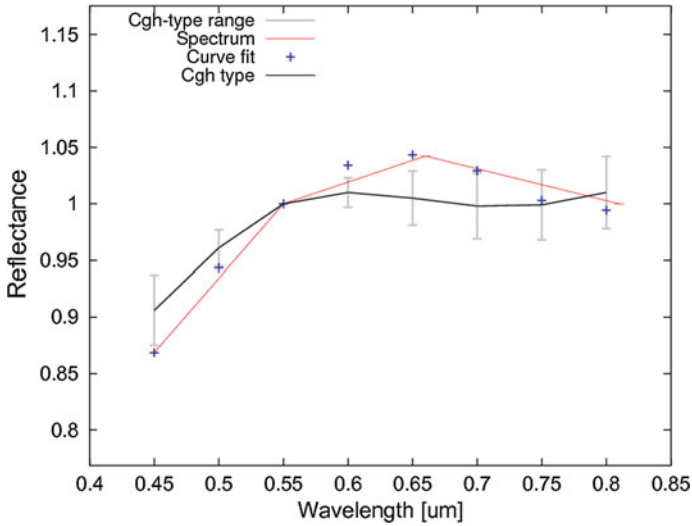


Fig. 7 Optical reflectance of 2014 WF201 matches Cg-type spectra

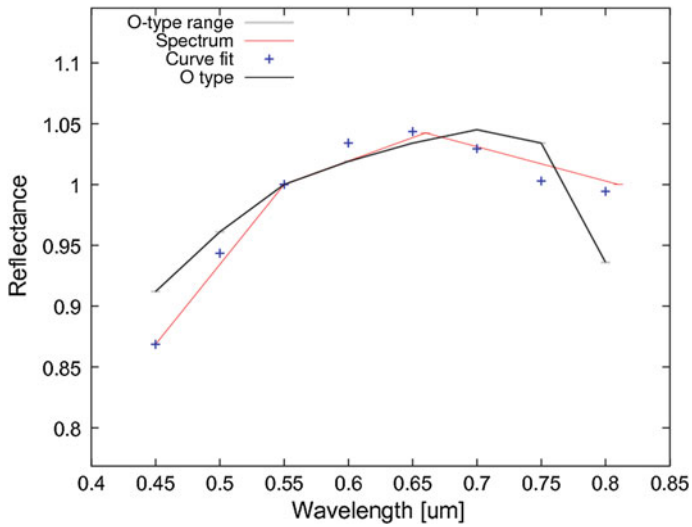


Fig. 8 Optical reflectance of 2014 WF201 matches O-type spectra

Color and Orbits

2014 AY28, 2014 WF201, 2015 TB25, 2015 VM64, 2015 VT64, 2015 XZ1, and 2016 GW221 are classified as C-type from the two color plots, and by comparing their relative reflectances with the observed spectra, they match various spectra (Cg,

Table 5 The 11 NEOs classified both using the two color plots and the comparison with the observed spectra

Asteroid	Classes	
	From Zeller et al. (1985)	From Popescu et al. (2012)
2014AY28	C	Cgh, Cg, O
2014EC	N/A	–
2014KS40	X	–
2014WF201	C	Cg, Cgh, O
2015FP	N/A	–
2015TB25	C	Cgh
2015VM64	C	Cgh, Ch
2015VT64	C	Cgh
2015XZ1	C	Cgh, C
2016EW1	C or S	O, Cg
2016GW221	C	Cgh

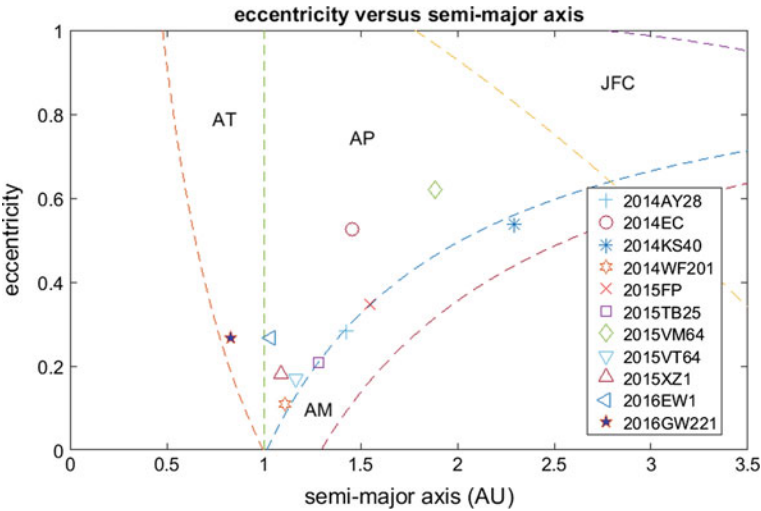


Fig. 9 Eccentricity versus semi-major axis

Cgh, Ch) of the C-complex class. In the (a, e) space, 4 of them (2014 AY28, 2014 WF201, 2015 TB25, and 2015 VT64) (Fig. 9) are Amor asteroids with $a < 2$. They are among those Amors in the inner region of the main belt that Dandy et al. (2003) found mixed with E-type and M-type asteroids. 2015 VM64, and 2015 XZ1 are C-type asteroids found among Apollo asteroids. 2014 EC could not be classified with the two color plots or by comparing its reflectance with observed spectra; however, it can be ruled out as S-type asteroid since it is an Apollo asteroid with $a > 2$ (Dandy et al. 2003). 2016 EW1 was classified either as C-type or S-type. Being in the region of Apollo asteroids and having $a < 1.5$, it would be more S-type than C-type.

Conclusion

The study of NEOs cannot be limited only to astrometry. It needs to be extended in the direction of physical characterization to know what NEOs are made of (their composition, and their structure). The more accurate method to accomplish this task is spectroscopy (optical and infrared). But being time consuming, and also expensive, the same task can be done with less expensive method: optical photometry, with a very inexpensive set of broadband filters (BVRI).

We were able to determine the color of 11 NEOs by combining different approaches. The first was the two color plots (Zellner et al. 1985) from color indices generated through photometry technique. The second approach was the comparison of NEOs relative reflectance normalized to V with the observed spectra in database. This second complements the first. Using the (a, e) space where different regions are populated by different asteroid families (Apollo, Amor, and Aten), and knowing the relationship that exists between these families and different colors of asteroids (Dandy et al. 2003), we were able to characterize the 11 NEOs observed with a 1.8 m telescope using Johnson-cousin optical filters.

We found that among the 11 NEOs, 7 are C-type asteroids or C-complex asteroids (Cg, Cgh, and Ch). There are 2014 AY28, 2014 WF201, 2015 TB25, 2015 VM64, 2015 VT64, 2015 XZ1, and 2016 GW221. Two could not be classified after the first approach, 2014 EC and 2015 FP. 2014 EC, being an Apollo asteroid with a > 2 , is more likely to be S-type. 2015 FP is an Amor asteroid, and is a C-type asteroid. In (a, e) space, 2014 KS40 falls in the region of Amor asteroids and has a > 2 . It is a probably a C-type NEO. Finally, 2016 EW1, classified either C or S in the two color plots, turns to be more S-type than C-type as it is an asteroid of Apollo family with a < 1.5 .

References

- Bottke, W. F., Morbidelli, A., Jedicke, R., Petit, J. M., Levison, H. F., Michel, P., et al. (2002). *Icarus*, 156, 399.
- Bus, S. J., Binzel, R. P. (2002a). *Icarus*, 158, 106.
- Bus, S. J., Binzel, R. P. (2002b). *Icarus*, 158, 146.
- Dandy, C. L., Fitzsimmons, A., Collander-Brown, S. J., Asher, D., Bailey, M. E. (2002). *Proceedings of Asteroids, Comets, Meteors*. ACM.
- Dandy, C. L., Fitzsimmons, A., & Collander-Brown, C. J. (2003). *Icarus*, 163, 363.
- Fedorets, G., Granvik, M., & Jedicke, R. (2017). *Icarus*, 285, 83.
- Froeschle, Ch., Hahn, G., Gnonezi, R., Morbidelli, A., & Farinella, P. (1995). *Icarus*, 117, 45.
- Landolt, A. U. (1992). *AJ*, 104, 340.
- Popescu, M., Birlan, M., & Nedelcu, D. A. (2012). *A&A*, 544, A130.
- Popescu, M., Licandro, J., Morate, D., de Leon, J., Nedelcu, D. A., Rebolo, R., et al. (2016). *A&A*, 591, A115.
- Rabinowitz, D. L. (1997). *Icarus*, 127, 33.
- Rabinowitz, D. L. (1998). *Icarus*, 134, 342.

- Schunova-Lilly, E., Jedicke, R., Veres, P., Denneau, L., & Wainscoat, R. J. (2017). *Icarus*, 284, 114.
- Tody, D. (1986). The IRAF data reduction and analysis system. In D. L. Crawford (Ed.), *Proceedings of SPIE Instrumentation in Astronomy VI* (Vol. 627, p. 733).
- Tody, D. (1993). IRAF in the nineties. In R. J. Hanisch, R. J. V. Brissenden, & J. Barnes (Eds.), *Astronomical data analysis software and systems II, A.S.P. Conference Series* (Vol. 52, p. 173).
- Tricarico, P. (2017). *Icarus*, 284, 416.
- Yoshida, F., Dermawan, B., Ito, T., Sawabwe, Y., Haji, M., Saito, R., et al. (2004). *PASJ*, 56, 1105.
- Zellner, B., Tholen, D. J., & Tedesco, E. F. (1985). *Icarus*, 61, 355.

The Vatican Observatory, Castel Gandolfo: 80th
Anniversary Celebration

Gionti, S. J., G.; Kikwaya Eluo, S.J., J.-B. (Eds.)

2018, XVI, 265 p. 103 illus., 66 illus. in color., Hardcover

ISBN: 978-3-319-67204-5